Synthesis and Characterization of Poly(oxytetramethylene) Ionene with 2,2′-Bipyridinium Units

Yuko Ikeda,* Takeshi Murakami, Yoshiaki Yuguchi, and Kanji Kajiwara

Faculty of Engineering and Design, Kyoto Institute of Technology, Matsugasaki, Sakyo, Kyoto 606, Japan

Received August 4, 1997; Revised Manuscript Received November 13, 1997

ABSTRACT: A novel ionene elastomer (DPI) consisting of 2,2′-bipyridinium units and poly(oxytetramethylene) (POTM) segments was synthesized by cationic polymerization of tetrahydrofuran followed by termination using 2,2′-bipyridine. The molecular mass between the ionic sites was ca. 10 000 g/mol. The DPI film displayed a high tensile strength up to 34 MPa and 540% elongation at break at 25 °C. The higher-order structure of the DPI film was investigated by thermal and dynamic mechanical analyses and by wide-angle X-ray diffraction and small-angle X-ray scattering (SAXS) measurements. The DPI film had a microphase-separated structure consisting of three phases of the POTM amorphous matrix, the POTM crystalline domain and the ionic domain at room temperature. The POTM crystalline domain was lamellar, and its spacing was ca. 270 Å. A new model was proposed to successfully account for the upturn of the scattering intensity toward zero angle in the SAXS profile of DPI at 65 °C, where two phases of the POTM amorphous matrix and the ionic domain were present. Namely, the cascade model for randomly branched *f*-functional polycondensates was adapted, where the inhomogeneous ionic domains consist of scattering points in a tree-like network. Each domain is described by the Debye−Bueche random-two-phase model, and the repulsive interaction takes place between the ionic domains. The size of the ionic domains was evaluated to be ca. 12 Å, and the mean interaction distance between the ionic domains was ca. 39 Å from the fitting of the model calculation to the observed SAXS profile. The system was in the vicinity of a gel point in terms of the cascade model, where the ionic domain serves as a physical cross-linking point.

Introduction

The introduction of ionic sites to polymer chains is known to change drastically the properties and the morphology of mother polymers in the field of polymer science. Among ionic polymers, the "ionomer" is referred to as the copolymers consisting of hydrophobic polymer segments and a small fraction of ionic sites. Generally, the ionic content of the ionomers is less than ca. 15 mol %. The physical properties of ionomers as high-performance materials have been extensively researched over the last few decades in the academic as well as the industrial fields.[1−7] Especially, the ionomer has attracted much attention as a thermoplastic elastomer.[6,7]

"Ionene", on the other hand, is classified as a cationic polymer, and some with lower cationic sites are included in the category of ionomer.[8] A living cationic polymerization produces the poly(oxytetramethylene) (POTM) ionenes from tetrahydrofuran (THF), and several studies revealed its unique physical properties.[9−25] For example, the ionene elastomer was synthesized from dimethylamino-terminated POTM and dihalides by the Menschutkin reaction, and the effect of counteranion on its mechanical properties and water vapor permeability was investigated.[9−12] The studies on the thermal reversibility[13] and the plasticization[14,15] of the POTM ionenes were also carried out for wide industrial applications. As the POTM ionene is a tailor-made material, various polymers can be prepared by changing a kind of amine for the termination reaction of polymerization of THF. Moreover, chain extension of bifunctional living POTM chains by α,ω-tertiary diamines affords a very direct and efficient pathway toward POTM ionenes, since quaternization of tertiary amines of high basicity and low steric hindrance by POTM oxonium end groups is a very fast, selective, and quantitative process.[16] Viologen-type POTM ionenes were synthesized by one-pot synthesis,[12,17,18] and the electrochromic,[19] photochromic,[17,19] and photomechanical behaviors[20] of resulting ionenes as functional elastomers were reported.

In this study, a new ionene elastomer was prepared according to Scheme 1, and the relationship between the physical properties and morphology was investigated. Especially, the effect of the crystalline phase of POTM segments on the mechanical properties was discussed because little research has been done on the crystallinity of POTM ionenes. Small-angle X-ray scattering (SAXS) was applied to analyze the morphology of the ionene quantitatively. This is because many reports have been directed toward a full understanding of the morphology of ionomers and several models have been proposed to account for the morphology of ionomers from the results of SAXS measurements.[21,26−28] Reviews of the works in this area are given in some articles.[2,3] Among several models, the combined modified Yarusso and Debye−Bueche model[28] was conceded to be adequate for the explanation of all ranges in the SAXS profile. However, we considered that it still remains to interpret the SAXS profile for the morphology of ionomers consisting of the amorphous matrix and the ionic aggregate. Thus, two alternative models are proposed to accurately fit the SAXS profile of the ionene elastomer prepared in this study. The Debye−Bueche random-two-phase model[29] and the cascade model for randomly branched *f*-functional polycondensates[30,31] are used separately and/or combined. To obtain the morphology consisting of the amorphous POTM matrix and the ionic aggregate, the sample was heated at 65 °C and

S0024-9297(97)01178-9 CCC: $15.00
Published on Web 02/04/1998

Scheme 1

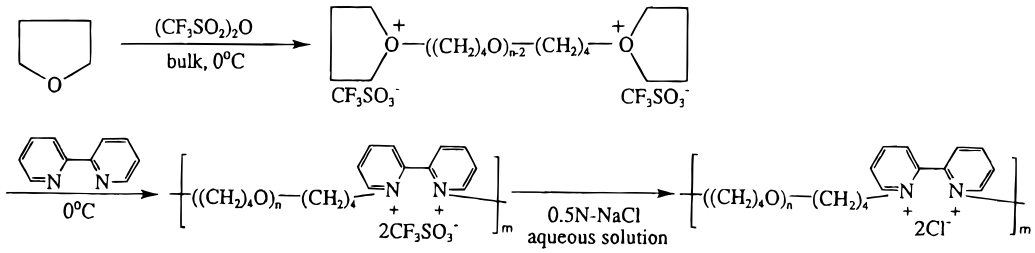

the SAXS measurement was carried out at this temperature.

Experimental Section

Reagents. Commercial THF was distilled three times over metallic sodium. Trifluoromethanesulfonic acid anhydride ($(CF_3SO_2)_2O$) was prepared from the acid (CF_3SO_3H, from Nacalai tesque) by distilling on P_2O_5,[9] just before use for the polymerization. 2,2′-Bipyridine was commercial origin and was purified by recrystallization from the petroleum ether solution. The solvents used in this study were purified by the conventional methods.

Synthesis of DPI. Scheme 1 shows the synthetic route of poly(oxytetramethylene) ionene (DPI) with 2,2′-bipyridinium units. Cationic living polymerization of THF (50 mL) was carried out by $(CF_3SO_2)_2O$ (1.1 mL, 0.130 mol/L) at 0 °C under dry nitrogen for 10 min. The termination reaction was conducted at 0 °C for 60 min by adding the THF solution of 2,2′-bipyridine (1.12 g) whose molar amount was equivalent to the initiator.[12,17] The resulting polymer was purified by reprecipitation from THF to water several times. The yield of DPI was ca. 39%. The exchange of counteranion in DPI from trifluoromethanesulfonate to chloride was conducted by pouring a 10% methanol solution of DPI into a 0.5 N sodium chloride aqueous solution three times at room temperature (rt). As a reference sample for DPI, a methoxy-terminated POTM (MT-PT) was also prepared by cationic polymerization of THF at 0 °C for 1 h and termination using a large excess of anhydrous methanol. The molecular mass and polydispersity of MT-PT were 19 000 g/mol and 1.9, respectively, which were evaluated by size-exclusion chromatography (SEC).

Molecular Characterization of DPI. The ^{1}H NMR spectrum was recorded on a Fourier transform high-resolution NMR spectrometer JEOL GX-400 (Nippon Denshi Co.) in CD_3-OD at 23 °C. Absorptions of two methylene groups of POTM chains (a and b) and protons of the bipyridinium ring (c, d, e, and f) are observed as shown in Figure 1. Signals indicative of side reaction are absent. FT-IR measurement was carried out on an infrared spectrometer FTIR-4100 (Shimadzu Corp.). IR (thin film): $\nu(CH_2)$ 2870, 2940 cm^{-1}; ν(CN of bipyridinium ring) + δ(CH) 1373 cm^{-1}; ν(C−O−C) 1116 cm^{-1}; δ(CH of the bipyridinium ring) 746 cm^{-1}.

SEC was conducted by using a Toso HLC-802UR high-performance liquid chromatograph with TSK-GEL TYPE GMH 4 column (polystyrene standards; solvent, THF; 40 °C). An elemental analysis was conducted at the Elemental Analysis Center of Kyoto University. Anal. Calcd for $C_{255}H_{504}O_{62}N_1Cl_{0.85}$: C, 66.24; H, 10.94; O, 21.65; N, 0.31; Cl, 0.77. Found: C, 65.48; H, 10.90; O, 21.55; N, 0.31; Cl, 0.65. From these results, the exchanged amount of counteranion from $CF_3SO_3^-$ to Cl^- was evaluated to be ca. 85%. The reduced viscosity was measured with an Ubbelohde viscometer at 30 ± 0.1 °C in a thermostated bath. The ionenes dissolved in chloroform and methanol. The reduced viscosity (η_{sp}/C) is plotted as a function of concentration (C (g/dL)). $\eta_{sp} = (\eta - \eta_0)/\eta_0$,where η and η_0 represent the viscosity of the solution and solvent, respectively.

Film Preparation. The film was prepared from its 3% chloroform solution by casting onto a Teflon mold at 50 °C and was subjected to drying under a reduced pressure. The thickness of the film was ca. 1 mm.

Dynamic Mechanical Analysis. The temperature dispersions of the dynamic modulus (E') and loss tangent (tan δ) of the polymer film were measured on a dynamic mechanical analyzer (DVE-V4 Rheospectra of Rheology Co., Ltd., Japan). The sample dimension was 15 mm × 5 mm × ca. 1 mm. The strain mode was used and the heating rate was 2 °C/min. The frequency was 10 Hz.

Tensile Test. Tensile measurement was carried out using a Tensile Tester TOM 200D (Shinko Thushin Kogyo Co. Ltd.) on ring-shaped dry samples at 25 °C. The extension speed was set to be 100 mm/min.

Differential Scanning Calorimetry. Differential scanning calorimetry (DSC) measurement was carried out on a Rigaku Thermoflex DSC-8230 under nitrogen. The sweep rate of temperature was 10 °C/min. The sample loaded was ca. 10 mg and the temperature range was −120 to +150 °C.

Thermogravimetric Analysis. The thermal stability of the ionene was studied on a thermogravimetric analyzer (Rigaku Co. Thermoflex No. 8002) at a heating rate of 10 °C/min in air.

Wide-Angle X-ray Diffraction. Wide-angle X-ray diffraction (WAXD)[32] measurement was carried out using a rotating-anode X-ray generator (Rigaku-Denki, RU-300) operated at 40 kV and 240 mA. CuKα X-ray beams monochromatized with a graphite monochromator were shone onto the specimen through a pinhole collimator of 0.5 mm in diameter. As an X-ray detector, the IP system (MAC Science, DIP-220) was utilized.

Small-Angle X-ray Scattering. SAXS measurement was carried out with the SAXES optics installed at BL-10C of the photon Factory, Tsukuba, Japan,[33] where an incident X-ray from synchrotron radiation was monochromatized to the wavelength of the X-ray (λ) = 1.488 Å with a double-crystal monochromator and then focused to the focal point with a bent focusing mirror. The scattered X-ray was detected by the one-dimensional position sensitive proportional counter of an effective length 160 mm positioned at the distance of about 1.0 m from the sample holder. The SAXS intensities were accumulated for an appropriate period of time to attain a sufficient S/N ratio. The exact camera distance was calibrated by using the diffraction peaks of the collagen fiber (the long period = 670 Å) at the sixth, ninth, and eleventh orders. Data were collected on a CAMAC system controlled by a NEC PC 9801 RX. The scattered intensities were corrected with respect to the variation of the incident X-ray flux by monitoring the beam with an ionizing chamber placed in front of the thermostated sample folder.

Transmission Electron Microscopy. An ultrathin film of DPI was prepared by using a microtome (LKB 4800 A ULTROTOME) in liquid nitrogen of LKB14800 CRYOKIT. The specimen was placed on a copper grid, which was coated with Folmbar and evaporated carbon in advance. Then, the specimen was exposed to the vapor of RuO_4. It was well dried under a vacuum, and the microscopic image was observed with a transmission electron microscope (JEOL JEM-100U). The accelerating voltage used here was 80 kV.

Results and Discussion

Synthesis of DPI. The chemical structure of DPI was confirmed from the ^{1}H NMR spectrum (Figure 1) and FT-IR spectrum of DPI. The molecular mass of the nonionic spacer was estimated as ca. 10 000 g/mol from the integral curve of the ^{1}H NMR. By elemental

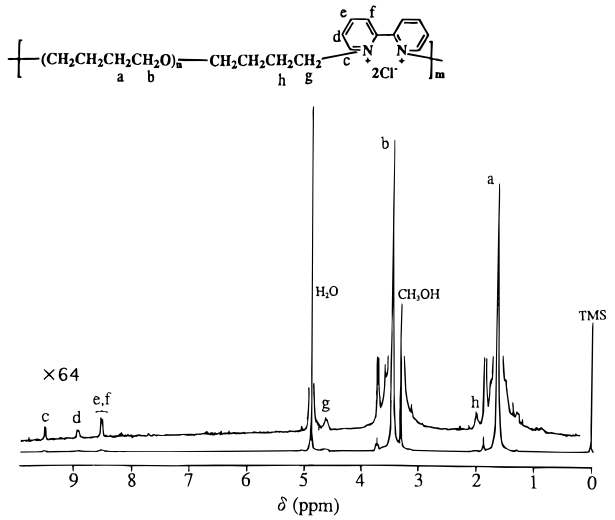

Figure 1. ^{1}H NMR spectra of DPI.

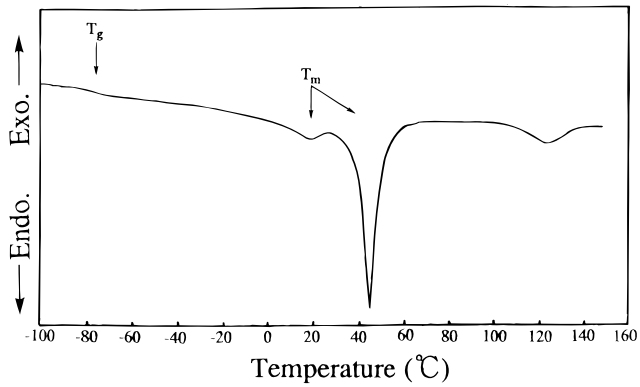

Figure 2. DSC curve of the DPI film.

analysis, the molecular mass of the POTM segment between the ionic sites was estimated as 10 700 g/mol, which is consistent with the ^{1}H NMR result. DPI was soluble in methanol, chloroform, THF, or benzyl alcohol and was not soluble in acetone, hexane, *N*,*N*′-dimethylformamide, or water. The viscosity of the methanol solution of DPI displayed the behavior of typical polymer electrolytes; i.e., the viscosity increased much with the decrease of the DPI concentration in the lower concentration region in methanol, whereas the viscosity of DPI in chloroform decreased continuously with the decrease of the DPI concentration, which is normally observed in nonelectrolytic polymers. The intrinsic viscosity of DPI in chloroform was estimated to be 2.23 dL/g. From the comparison of the intrinsic viscosity of DPI with that of MT-PT (0.28 dL/g), the chain extension reaction between 2,2′-bipyridine and POTM living dications was concluded to progress well under the present reaction conditions.

Thermal Properties of the DPI Film. A DPI film, whose thickness was ca. 1 mm, was prepared by casting the chloroform solution of DPI. The film was optically clear and light-brown. The DSC curve of the DPI film is illustrated in Figure 2. The glass transition temperature (T_g) of the POTM amorphous phase was detected at ca. −79 °C, and the large endothermic peak due to the melting of the POTM crystalline phase appeared at ca. 42 °C. An additional peak was observed at ca. 125 °C, which could be attributed to the melting or the softening of ionic domains. The heat of fusion of the phase transition peak of the ionic domains was ca. 0.95 cal/g. The observed transition temperatures of the POTM segments were very similar to those of MT-PT, whose T_g and melting temperature (T_m) were ca. −81 °C and ca. 43 °C, respectively. As the DPI film was optically clear at rt, the microphase separation seems to have taken place at rt, where the amorphous POTM segments, the crystalline phase of POTM segments, and the ionic aggregated domains are suggested to be present by DSC.

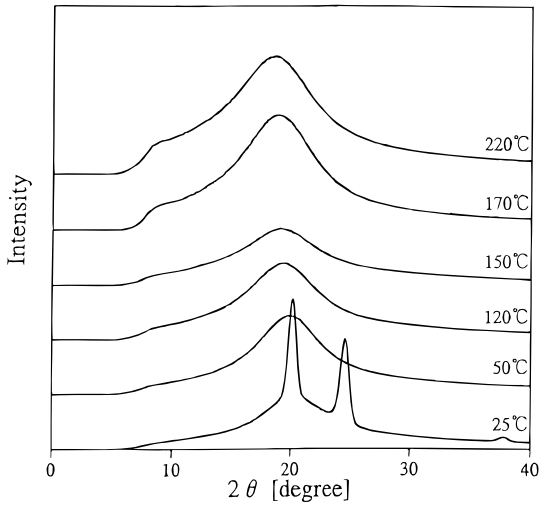

Figure 3. Temperature dependence of WAXD profiles of theDPI film.

WAXD measurements revealed the crystallization of POTM segments more clearly. The profiles of the WAXD pattern of the DPI film are shown in Figure 3. In the profile measured at 25 °C, the diffraction peaks were clearly detected at the scattering angles of 20.0° and 24.6°. A weak scattering ring was observed at 37.6°. The angles of these peaks are found to consistent with those (19.9°, 24.0°, 37.6°) reported in the reference[34] and with those (19.8°, 24.4°, 37.7°) observed from a commercial hydroxyl-terminated POTM (the molecular mass is ca. 2000 g/mol). Therefore, the scattering peaks of the DPI film at 20.0°, 24.6°, and 37.6° are attributed to the (020), (110), and (130) reflections of the POTM crystals, respectively. These reflections disappeared at a temperature higher than 50 °C, as shown in Figure 3, suggesting that the POTM crystal melts at around 50 °C. This phenomenon was also confirmed by the polarized microscopic observation under crossed Nicol prisms, where the anisotropy due to the crystalline phase of POTM segments at 25 °C was lost at 50 °C to become isotropic. Thus, the POTM phase was amorphous at temperature regions higher than 50 °C.

Interestingly, the decomposition temperature of DPI was higher than that of MT-PT. The temperatures of 5 wt % loss and 10 wt % loss for DPI were ca. 344 °C and ca. 350 °C, whereas those of MT-PT were ca. 283 °C and ca. 312 °C, respectively. The reason is not yet clear, but it may be due to the higher molecular mass of DPI than of MT-PT.

Mechanical Properties of the DPI Film. The stress−strain curve of the DPI film at 25 °C is illustrated in Figure 4. The modulus remains low until ca. 300% elongation, and its rapid increase was observed at a higher elongation than 300%. The tensile strength at break was 34.4 MPa, and the elongation at break was 540%. The large increase of the modulus at higher

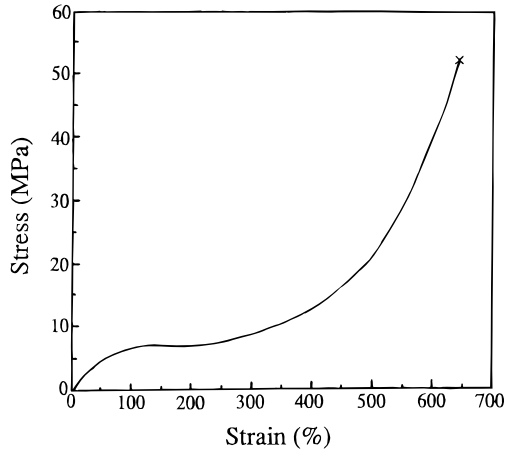

Figure 4. Stress−strain curve of the DPI film at 25 °C.

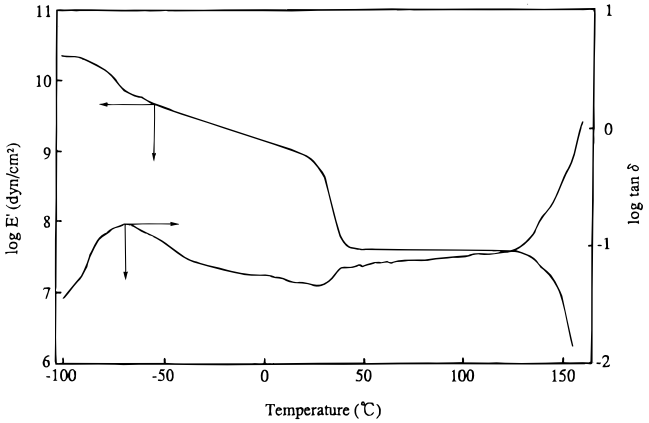

Figure 5. Temperature dependence of E' and tan δ of the DPI film.

strains could be ascribed to the strain-induced further crystallization of the POTM segments. The ionic sites are assumed to function as physical cross-linking sites in analogy with similar tensile behaviors observed in many ionomers and ionenes. Additionally, the crystalline region of POTM segments much influences the mechanical properties of this DPI film. Compared with the reported 100% modulus of the ionene with POTM soft segment whose molecular mass was ca. 2000 g/mol and 4,4′-bipyridinium,[21] the 100% modulus of the DPI film was about 3 times larger. This difference is explained by the reinforcement effect of the POTM crystalline domain on the tensile properties of DPI.

The temperature dispersions of E' and tan δ are shown in Figure 5. The T_g and the T_m of the POTM segments were detected at ca. −74 °C and ca. 20 °C, respectively. The rubbery plateau appeared after the decrease of the E' around T_m and continues to ca. 130 °C, which corresponds to the softening point of DPI. In the rubbery plateau region, the domains composed of the aggregated ionic units of DPI functioned as physical cross-linking sites. Thus, the softening corresponds to the phase transition of the ionic domains, which was also confirmed by DSC. E' at 25 °C was 6.8×10^8 dyn/cm^2, and E' at 65 °C was 4.4×10^7 dyn/cm^2. This difference is accounted for by the melting of the crystalline region of POTM segments. The crystalline region is considered to act as an effective reinforcing filler.

Morphology of the DPI Film. The DSC and the dynamic mechanical analysis (DMA) results indicate that the DPI film prepared in this study consists of three

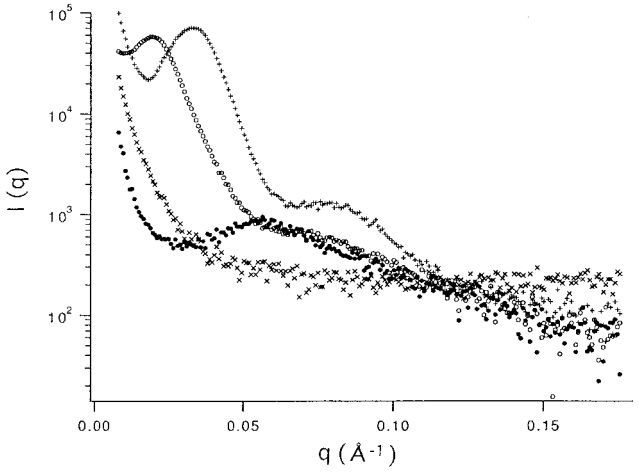

Figure 6. Observed SAXS profiles from the DPI film and the MT-PT film at rt and 65 °C: (○) DPI at rt; (●) DPI at 65 °C; (+) MT-PT at rt; (×) MT-PT at 65 °C.

phases at rt. To elucidate the morphology of the DPI film in more detail, SAXS was observed from the DPI film at rt and at 65 °C, respectively. As a reference, MT-PT, which has no ionic sites, was also subjected to the SAXS measurements. The SAXS profiles are illustrated in Figure 6. By heating, the SAXS peaks disappeared from the MT-PT film, whereas a single broad peak remained at 65 °C in the DPI film. The broad peak at 65 °C is considered to be due to the ionic domains in the amorphous POTM matrix.

SAXS has been applied to analyze the morphology of ionomers, and several morphological models have been presented to explain their typical SAXS profiles. Here, the typical SAXS profile from ionomers is characterized by a single peak with a Bragg spacing of 20−100 Å and a strong upturn in the intensity at near-zero angle. However, no proposed models[2,3] afforded a consistent description to the characteristics of the typical SAXS profile from ionomers till 1988. Cooper et al.[28] have succeeded in fitting the SAXS profile from a nickel-neutralized sulfonated polystyrene with a modified Yarusso−Cooper model combined with the Debye−Bueche random-two-phase model.[29] In all fairness, however, Cooper et al. conceded that the Debye−Bueche model was not the only possible explanation for the upturn of the SAXS profile at the scattering vector (q) $\rightarrow$ 0 in their publication. Thus, an alternative model was proposed in this study to describe quantitatively the SAXS profile from the ionic domains in the amorphous polymer matrix.

At 65 °C. As shown in Figure 6, a single broad peak was observed in the SAXS profile of the DPI film at 65 °C. Generally, in the case of a polymer containing ionic sites, the scattering intensity ($I(q)$) as a function of q is expressed in terms of the product of the scattering from the polymer chain itself ($P(q)$) and the interference due to the repulsive interaction between the ionic domains formed in the polymer matrix ($S(q)$).

$$I(q) \approx P(q)\, S(q) \tag{1}$$

$$q = 4\pi \sin(\theta/2)/\lambda \tag{2}$$

where λ is the wavelength of X-ray and θ is the scattering angle. $S(q)$ is approximately given as

$$S(q) \approx 1/(1 + c \exp(-\xi^2 q^2)) \tag{3}$$

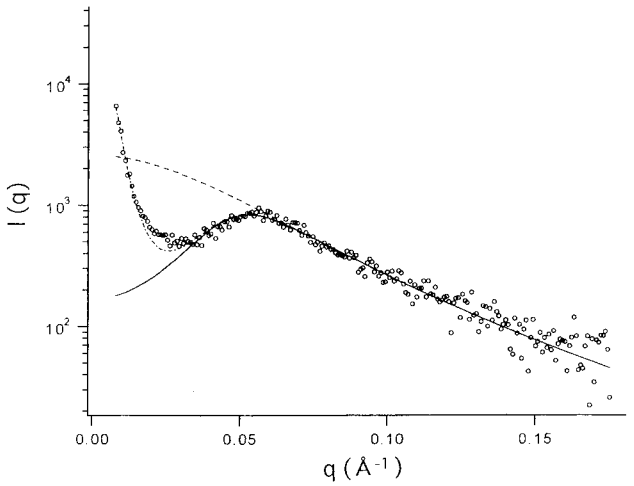

Figure 7. Observed SAXS profile (○) from the DPI film at 65 °C and the SAXS profile fitted by using the linear sum of $P(q)$ $S(q)$ (eq 1), where $P(q)$ is Debye−Bueche type (eq 5), $S(q)$ is eq 3, and the excess scattering represented by Debye−Bueche type (one-dot line). Here the $P(q)$ is indicated by a dotted line, and $P(q)$ $S(q)$, by solid line.

which assumes a Gaussian type interaction potential specified by the correlation length (ξ). Here, c is an adjustable parameter to take into account the strength of interaction. Two approaches were attempted in this study to reproduce the SAXS profile of the DPI film at 65 °C in terms of eq 1. Two morphological models are considered, and the preference will be discussed.

In model I, the Debye−Bueche random-two-phase model[29] was employed to formulate $P(q)$ in eq 1. The inhomogeneous structure consisting of two phases with a smooth boundary is specified by the following correlation function with the correlation length (a).

$$\gamma(r) \approx \exp(-r/a) \tag{4}$$

$\gamma(r)$ represents the distance correlation between any two points separated by a distance (r), where "a" is a measure of the extent of the inhomogeneity. By Fourier transformation of the correlation function, a scattering intensity is calculated as

$$I(q)_{\mathrm{D-B}} \approx 1/(1 + a^2q^2)^2 \tag{5}$$

The correlation length is estimated by fitting this scattering function directly to the experimental data. Assuming two inhomogeneous domains specified by the respective correlation length in the Debye−Bueche formula (eq 4), the observed SAXS profile is fitted to the sum of eqs 1 and 5 when $P(q)$ in eq 1 is assumed to be given by eq 5. Smaller heterogeneous domains are considered to be composed of ion clusters and yield the SAXS profile described by eq 1, as shown by a solid line in Figure 7. The total composed profile is shown by a one-dot line in Figure 7. Although the calculated profile reproduces well the observed trend especially in the region of $q > 0.05$ Å^{-1}, it fails to cope with the inflection at lower q region ($q = 0.02 \sim 0.03$ Å^{-1}) (see Figure 7). Here the second Debye−Bueche component was introduced in order to take account of the upturn scattering at $q \rightarrow 0$. Larger heterogeneous domains could be constituted of "pseudocrystalline" domains, which are depicted to have no crystalline structure yielding WAXD peaks at high temperatures, but form a crystalline phase at lower temperatures. It is also interpreted as the high-density region remaining that is not completely melted and has a low enough mobility to prevent electrostatic interactions from taking place.[35,36] Namely, no electrostatic interaction is expected between the larger heterogeneous component, so that the $S(q)$ factor was not taken into account in this region. By using model I, the larger domain is specified by the heterogeneous structure of ca. 200 Å in size, while the smaller domain is as small as 15 Å. Cooper et al.[28] discussed the zero-angle scattering related to the neutralizing cation of the polystyrene ionomer. They speculated that the zero-angle scattering was due to an inhomogeneous distribution of isolated ionic groups in the matrix and applied the Debye−Bueche random-two-phase model to the data. In this study, however, the chloride anion was not assumed to be isolated in the POTM matrix.

An alternative model (model II) is based on the cascade process for randomly branched f-functional polycondensates.[30,31] The model is composed of the small heterogeneous domains formed by ion clusters, which are distributed over the space (polymer matrix) in a random fashion described by the cascade process. The cascade process for randomly branched f-functional polycondensates yields a tree-like network, where each node (scattering unit) is constituted of ion clusters. The scattering intensity for the simple cascade model is calculated as

$$I(q)_C \approx (1 + \alpha\phi)/[1 - (f - 1)\alpha\phi] \tag{6}$$

where $\phi = \exp(-b^2q^2/6)$, α is the extent of reaction, f is the number of the functional group, i.e., the functionality of cross-linking, and b^2 corresponds to the mean-square distance between adjacent scattering units. The scattering units are assumed to be point-like in eq 6. The shape upturn of the scattering intensity at $q \rightarrow 0$ is expected upon gelation from eq 6, which was also confirmed experimentally. An ionomer can be considered as a kind of physical network when the cross-linking points are supposed to be composed of ion clusters. The heterogeneous domains of ion clusters are tied with neutral polymeric chains and form a network. When the cascade model for randomly branched f-functional polycondensates is applied, the scattering units should be replaced with the heterogeneous domains specified by the Debye−Bueche correlation function. Thus, eq 6 is rewritten for the model of the heterogeneous domains forming the cascade network as

$$I(q) \approx I(q)_{\mathrm{D-B}}(1 + \alpha\phi)/[1 - (f - 1)\alpha\phi] \tag{7}$$

Here f denotes the average number of ties from one heterogeneous domain. When the electrostatic repulsion is taken into account, eq 7 is further modified as

$$I(q) \approx [I(q)_{\mathrm{D-B}}(1 + \alpha\phi)/[1 - (f - 1)\alpha\phi]]S(q) \tag{8}$$

The observed SAXS profile from DPI at 65 °C was analyzed in terms of the cascade model. As shown in Figure 8, a good fitting was achieved in all q regions between the observed SAXS data and the values calculated according to eq 8. From the parameters obtained by the best fitting, the size of the ionic domains and their interaction distance were estimated to be ca. 12 Å and ca. 39 Å, respectively. It is interesting to note that the DPI film is suggested to be in the vicinity of the gel point from the viewpoint of the cascade model, because the product of α and $(f - 1)$ was found to be

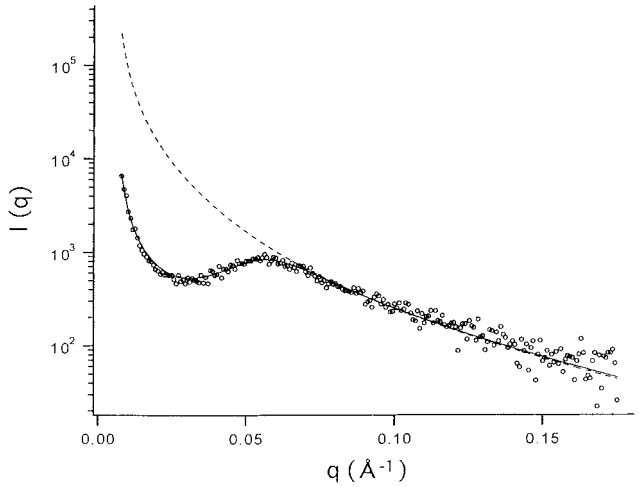

Figure 8. Observed SAXS profile (○) from the DPI film at 65 °C and the SAXS profile (solid line) fitted by using the modified cascade model with the interaction effect (eq 8). Here the dotted line denotes the profile without the interaction effect.

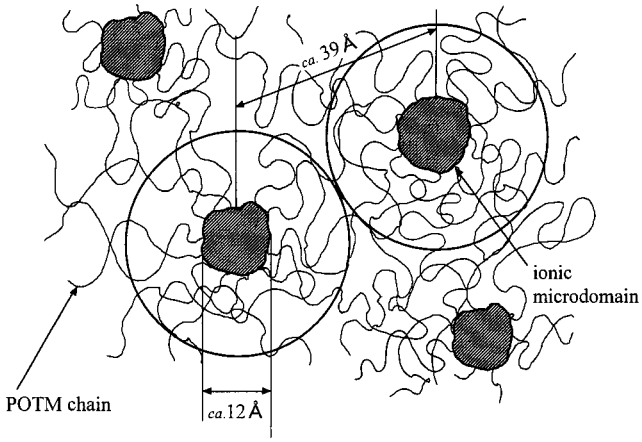

Figure 9. Morphology of the DPI film at 65 °C.

almost 1.[31] The possible model of the morphology for the DPI film at 65 °C is illustrated in Figure 9.

Assuming the Gaussian network, the molecular weight of the interval chain between cross-links, i.e., ionic domains (M_c), can be estimated approximately from the elastic modulus of the DPI film at 65 °C with the aid of the classical theory of rubber elasticity.[37]

$$E = 3\rho RT/M_c \tag{9}$$

where E and ρ denote the dynamic modulus and the polymer density, respectively. The value of 0.982[38] was adopted for ρ. The M_c of the DPI film at 65 °C was estimated to be 2010 using the following equation.[23,25,39] The end to end distance (L) of POTM (N monomeric units) segments connecting neighboring ionic domains was calculated from

$$L = [C_\infty N \sum n_i l_i^2]^{1/2} \tag{10}$$

where the parameter l_i is related to the i th bond length: l(C−C) = 1.53 Å, l(C−O) = 1.43 Å. The POTM characteristic ratio (C_∞) taken from the literature is 5.8.[39,40] The distance between the ionic domains calculated by eq 9 was ca. 38 Å and was almost identical with that (ca. 39 Å) by SAXS measurement. This result

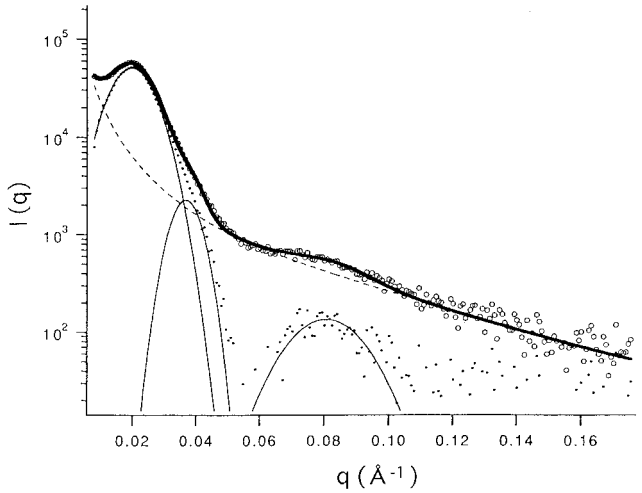

Figure 10. Observed SAXS profile (○) from the DPI film at rt and the SAXS profile (wide solid line) calculated by eq 7 with the three peaks (solid line) added in terms of the Gaussian function. Here the dotted line is calculated without adding peaks.

strongly supported model II to be pertinent for a detailed analysis of the DPI's morphology at 65 °C.

A good agreement in the interdomain distance evaluated by two independent methods indicates that no chain extension effect is observed on the POTM segments. As pointed out by Feng and Wilkes,[39] the expansion of the POTM chain in similar ionene polymers becomes more marked with the decrease of the molecular mass of a POTM soft segment. However, this phenomenon was observed for the ionene with POTM molecular mass under ca. 5000 g/mol. In this study, the molecular mass between ionic sites was ca. 10 000 g/mol, which would be large enough to maintain the unperturbed conformation, as observed as a chain conformation between the ionic domains.

At Room Temperature. The SAXS profiles of DPI and MT-PT at rt are shown in Figure 6. The Bragg spacings (d) were calculated from the position of the scattering peaks (q_{peak}) by using following equation.

$$d = 2\pi/q_{peak} \tag{11}$$

The Bragg spacings for the DPI film and the MT-PT film were estimated as ca. 270 Å and ca. 190 Å, respectively, which reflect the long range ordering of the POTM crystalline phase.

The SAXS profile of DPI at rt was analyzed further in terms of the morphological model developed to be consistent with the observed results at 65 °C. At rt, the crystallization will take place in the POTM phase, for which the ionic domains remain practically unchanged. Thus, the SAXS profile of DPI at rt is suppressed to be composed of the contributions from ionic domains and crystalline phases. The scattering from the ionic domain can be dealt with as considered in the previous section except for the electrostatic repulsion, which will be shielded by the crystalline phases. Applying eq 7 for the contribution from the ionic domains (a dotted line in Figure 10), the contribution from the crystalline phases emerges, as shown by dots in Figure 10. Since the crystalline phase is not well organized, the structural fluctuation is taken into account by assuming the broadening of the diffraction peak in terms of the Gaussian function. The fitted results are shown by three thin solid peaks at q = 0.21,

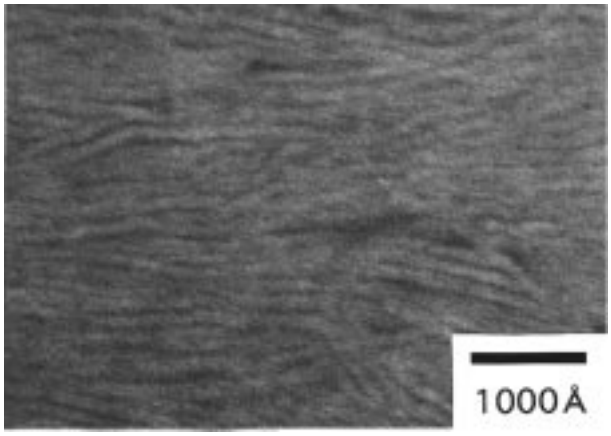

Figure 11. TEM photograph of the DPI film at rt.

0.42, and 0.82 $Å^{-1}$, respectively. The total composite scattering profile (a thick solid line in Figure 10) represents well the observed SAXS data. The ratio of these peak intensities was 1/2/4, which suggests that the POTM crystalline phase has a lamellar structure. Generally, the SAXS profile from the lamellar structure has four peaks whose intensity ratio is 1/2/3/4. However, the SAXS profile composed of three peaks with the ratio of 1/2/4 (where the third peak is missing) was also observed and analyzed as a lamella in the study on triblock copolymers.[41]

The presence of the lamellar structure was confirmed by the transmission electron microscopy (TEM) observation. The TEM photograph in Figure 11 clearly shows the lamellar structure. The distance between the lamellae is estimated to be ca. 260 Å, which is almost equal to that (ca. 270 Å) evaluated by SAXS measurement. The lamellae are visualized as dispersed continuously in the matrix. No information on the ionic aggregates at rt could be obtained by TEM. However, the ionic sites should be an important factor to give the characteristic morphology of DPI at rt, as suggested in the results of tensile properties.

Conclusion

A novel ionene elastomer (DPI) was synthesized by cationic polymerization of THF followed by termination using 2,2′-bipyridine. Thus, DPI consisted of 2,2′-bipyridinium units and POTM segments. The molecular mass between the ionic sites was ca. 10 000 g/mol. The DPI film, which was prepared by casting the chloroform solution of DPI, displayed a high tensile strength up to 34 MPa and 540% elongation at break at 25 °C. The higher-order structure of the DPI film was investigated by thermal and dynamic mechanical analyses and by WAXD and SAXS measurements. This POTM ionene was found to have a microphase-separated structure consisting of three phases of the POTM amorphous matrix, the POTM crystalline domain, and the ionic domain at rt. The POTM crystalline domain was lamellar, and its spacing was ca. 270 Å, which was evaluated by SAXS.

Two alternative models were proposed to account for the upturn of the scattering intensity toward zero angle in the SAXS profile of DPI at 65 °C. Since no crystalline phase is present at 65 °C, DPI is considered to consist of two phases of the POTM amorphous matrix and the ionic domain. The SAXS profile of DPI at 65 °C is thus dominated by the ionic domains of high electron density due to the contrast. In model I, we consider two distinct inhomogeneous domains specified by the Debye−Bueche correlation function (eq 4). A smaller inhomogeneous domain is an ionic domain composed of ion clusters, whereas a larger inhomogeneous domain is supposed to represent the incompletely melted POTM crystalline phase. The ionic domains interact electrostatically with each other, revealing the influence peak in the SAXS profile. The size of the smaller domain (the ionic domain) is ca. 15 Å and that of the larger domain is estimated as ca. 200 Å from the fitting of the model calculation with the observed SAXS profile.

The cascade model for randomly branched *f*-functional polycondensates was adapted for model II, where the inhomogeneous ionic domains consist of the scattering points in the tree-like network. Each domain is described by the Debye−Bueche random-two-phase model, and the repulsive interaction takes place between the ionic domains. The size of the ionic domains was evaluated to be ca. 12 Å and the mean interaction distance between the ionic domains was ca. 39 Å from the fitting of the model calculation to the observed SAXS profile. No large inhomogeneous domain is necessary to account for the upturn of the scattering intensity toward zero angle in this model (model II). Here ionic domains are distributed over the amorphous polymer matrix in such a way that the space correlation is described by the tree-like network formulated according to the cascade model for randomly branched *f*-functional polycondensates. It is also interesting note that the system is in the vicinity of a gel point in terms of the cascade model, where the ionic domain serves as a physical cross-linking point. A better fitting with the observed SAXS profile indicates that model II is more probable to describe the morphology of DPI. However, it should be emphasized that no direct proof is available to discard the large inhomogeneous domain in model I.

Acknowledgment. We thank Prof. Dr. S. Kohjiya, Dr. S. Murakami, and Mr. M. Ohara of Kyoto University and Dr. H. Urakawa of Kyoto Institute of Technology for their help in the WAXD, SAXS, and TEM measurements and for their valuable discussions. Financial support of this study by Tokuyama Science Foundation to Y.I. is gratefully acknowledged.

References and Notes

(1) Otocka, E. P. *J. Macromol. Sci., Rev. Macromol. Chem.* **1971**, *C5* (2), 275−294.
(2) Tant, M. R.; Wilkes, G. L. *J. Macromol. Sci., Rev. Macromol. Chem. Phys.* **1988**, *C28* (1), 1−63.
(3) Maurtz, K. A. *J. Macromol. Sci., Rev. Macromol. Chem. Phys.* **1988**, *C28* (1), 65−98.
(4) Fitzgerand, J. J.; Weiss, R. A. *J. Macromol. Sci., Rev. Macromol. Chem. Phys.* **1988**, *C28* (1), 99−185.
(5) Jerome, R.; Broze, G. *Rubber Chem. Technol.* **1988**, *58*, 223−242.
(6) Hara, M.; Sauer, J. A. *J. Macromol. Sci., Rev. Macromol. Chem. Phys.* **1994**, *C34* (3), 325−373.
(7) Ikeda, Y. *J. Soc. Rubber Ind. Jpn.* **1995**, *68*, 213−225.
(8) Meyer, W. H.; Dominingez, L. In *Polymer Electrolyte Reviews-2*; MacCallum, J. R., Vincent, C. A., Eds.; Elsevier Applied Science: London & New York, 1989; pp 191−227.
(9) Kohjiya, S.; Ohtsuki, T.; Yamashita, S. *Makromol. Chem. Rapid Commun.* **1981**, *2*, 417−420.
(10) Kohjiya, S.; Ohtsuki, T.; Yamashita, S.; Hashimoto, T. *Bull. Chem. Soc. Jpn.* **1990**, *63*, 2089−2093.
(11) Kohjiya, S.; Ohtuki, T.; Yamashita, S. *Makromol. Chem.* **1990**, *191*, 397−403.
(12) Kohjiya, S.; Yamashita, S. *Kautschuk Gummi. Kunstst.* **1991**, *44*, 1128−1132.
(13) Leir, C. M.; Stark, J. E. *J. Appl. Polym. Sci.* **1989**, *38*, 1535−1547.

(14) Feng, D.; Venkatesshwaran, L. N.; Wilkes, G, L.; Leir, C. M.; Stark, J. E. *J. Appl. Polym. Sci.* **1989**, *37*, 1549−1565.
(15) Venkateshwaran, L. N.; Leir, C. E.; Wilkes, G. L. *J. Appl. Polym. Sci.* **1991**, *43*, 951−966.
(16) Cunliffe, A. V.; Richards, D. H.; Robertson, F. *Polymer* **1981**, *22*, 108−116.
(17) Kohjiya, S.; Hashimoto, T.; Yamashita, S.; Irie, M. *Chem. Lett.* **1985**, 1497−1500.
(18) Kohjiya, S.; Hashimoto, T.; Yamashita, S. *J. Appl. Polym. Sci.* **1992**, *44*, 555−559.
(19) Hashimoto, T.; Kohjiya, S.; Yamashita, S.; Irie, M. *J. Polym. Sci., Polym. Chem.* **1991**, *29*, 651−655.
(20) Kohjiya, S.; Hashimoto, T.; Yamashita, S. *Macromol. Chem. Rapid Commun.* **1989**, *10*, 9−12.
(21) Hashimoto, T.; Sakurai, S.; Morimoto, M.; Nomura, S.; Kohjiya, S.; Kodaira, T. *Polymer* **1994**, *35*, 2672−2678.
(22) Grassl, B.; Galin, J.-C. *Macromolecules* **1995**, *28*, 7035−7045.
(23) Feng, D.; Wilkes, G. L.; Lee, B.; McGrath, J. E. *Polymer* **1992**, *33*, 526−535.
(24) Grassl, B.; Meurer, B.; Scheer, M.; Galin, J.-C. *Macromolecules* **1997**, *30*, 236−245.
(25) Grassl, B.; Mathis, A.; Rawiso, M.; Galin, J. −C. *Macromolecules* **1997**, *30*, 2075−2084.
(26) MackNight, W. J.; Taggart, W. P.; Stein, R. S. *J. Polym. Sci., Polym. Symp. Ed.* **1974**, *45*, 113−128.
(27) Eisenberg, A.; Hird, B.; Moore, R. B. *Macromolecules* **1990**, *23*, 4098−4107.
(28) Ding, Y. S.; Hubbard S. R.; Hodgson, K. O.; Register, R. A.; Cooper, S. L. *Macromolecules* **1988**, *21*, 1698−1703.
(29) Debye, P.; Bueche, A. M. *J. Appl. Phys.* **1949**, *20*, 518−525.
(30) Kajiwara, K.; Burchard, W.; Gordon, M. *Br. Polym. J.* **1970**, *2*, 110−115.
(31) Kajiwara, K. *J. Chem. Phys.* **1971**, *54*, 296−300.
(32) Murakami, S.; Nishikawa, Y.; Tsuji, M.; Kawaguchi, A.; Kohjiya, S.; Cakmak, M. *Polymer* **1995**, *36*, 291−297.
(33) Ueki, T.; Hiragi, Y.; Izumi, Y.; Tagawa, H.; Kataoka, M.; Muroga, M.; Matsushita, T.; Amemiya, Y. *Photon Factory Rep.* **1983**, *IV*, 70.
(34) Imada, K.; Miyakawa, T.; Chatani, Y.; Tadokoro, H.; Murahashi, S. *Macromol. Chem.* **1965**, *83*, 113−128.
(35) Russell, T. P.; Koberstein, J. T. *J. Polym. Sci., Polym. Phys. Ed.* **1985**, *23*, 1109−1115.
(36) Ryan, A. J.; Bras, W.; Geoffrey, R. M.; Derbyshire, G. E. *Polymer* **1994**, *35*, 4537−4544.
(37) See, for example: Flory, P. J. *Principles of Polymer Chemistry*; Cornell University Press: Ithaca, NY, 1953.
(38) Bowman, I.; Brown, D. S.; Wetton, R. E. *Polymer* **1969**, *10*, 715−717.
(39) Feng, D.; Wilkes, G. L. *Macromolecules* **1991**, *24*, 6788−6790.
(40) Brandrup, J.; Immergut, E. H. *Polymer Handbook*, 2nd ed.; John Wiley & Sons: New York, 1975; p IV-45.
(41) Matsushita, Y.; Momose, H.; Yoshida, Y.; Noda, I. *Polymer* **1997**, *38*, 149−153.

MA971178H